Maximum Observation of a Target by a Slower Observer in 3-Dimensions

Isaac E. Weintraub *, Alexander Von Moll †, and Eloy Garcia ‡
Air Force Research Laboratory, Wright-Patterson AFB, OH 45433, USA

Meir Pachter§
Air Force Institute of Technology, Wright-Patterson AFB, OH 45433, USA

Nomenclature

$\mathscr{C}$ = termination set
$\mathbf{f}$ = system nonlinear dynamics
$\mathscr{H}$ = Hamiltonian
J = objective cost functional
m = terminal manifold
t = time, [sec]
x_i = x-position of an agent, i, [normalized-length]
$\mathbf{u}$ = controls of the dynamic system
$\mathbf{x}$ = states of the dynamic system
y_i = y-position of an agent, i, [normalized-length]
z_i = z-position of an agent, i, [normalized-length]
γ_i = flight path angle for an agent, i, [rad]
λ_x = costate for a state, x
$\boldsymbol{\lambda}$ = vector of costates
μ = speed ratio
ψ_i = heading angle for an agent, i, [rad]

Subscripts
0 = initial time
f = final time
O = Observer
T = Target

Superscripts
$*$ = optimal value

I. Introduction

In this paper we consider the observation of a faster, non-maneuvering, target by a slower observer in 3-dimensional (3-D) Cartesian space, rather than in the plane. The observation problem is commonly referred to as Intelligence, Surveillance, and Reconnaissance (ISR) [1–3]. One goal of an ISR platform is the observation of a target, whether it be moving or stationary.

Observation of a slower ground vehicle by a single or team of faster aerial platforms has been considered [4–10]. Shaferman and Shima considered the tracking problem of a ground moving target in an urban terrain, with and without airspace limitations [4]. In their paper, they considered the task of tracking the ground vehicle by either a single or team

*Electronics Engineer, Aerospace Vehicles Technology Assessment and Simulations, Air Force Research Laboratory, Wright-Patterson AFB, OH 45433, AIAA Senior Member

†Electronics Engineer, Control Science Center of Excellence, Air Force Research Laboratory, Wright-Patterson AFB, OH 45433

‡Electronics Engineer, Control Science Center of Excellence, Air Force Research Laboratory, Wright-Patterson AFB, OH 45433, AIAA Member

§Professor, Department of Electrical and Computer Engineering, Air Force Institute of Technology Wright-Patterson AFB, OH 45433, AIAA Senior Member

of unmanned air vehicles. In order to handle the computational complexity from numerous mobile agents, Shaferman and Shima made use of an Evolutionary Algorithm (EA) to find optimal strategies for the multiple UAVs. In another work, He, Bachrach, and Roy considered a quad-rotor utilizing a downward-pointing camera capable of tracking a ground vehicle restricted to a road network [5]. He et al. considered a Bayesian approach for tracking the targets and demonstrated their approach in simulation and on hardware. In [6], sensor coverage effectiveness for a single mobile target and a group of mobile sensors was investigated. In their work, the authors described a connection between numbers of searchers and the amount of searcher motion. In [7], the coverage of a mobile sensor network resulting from continuous movement of sensors was studied. In their work, the authors took a game theoretic approach and obtained the optimal mobility strategy for sensors and intruders. In his master's thesis, Livermore considered an ISR platform equipped with a gimbaled camera which allowed the ISR platform to observe a ground target at various aspect angles [8]. In [9], Zhang and Hwang proposed a strategy for a single fixed-wing aircraft to tracking multiple mobile ground targets using recursive Bayesian estimation. Garnett and Flenner presented a problem consisting of a faster ISR platform and slower target in 2-D where the goal was to maximize the information was shared between two UAVs [10]. Because of the model complexity, they required the use of a nonlinear program solver to numerically find the optimal control strategies for the ISR platform which maximized the information shared between the two UAVs.

Differential games which posed the surveillance of an evading player were considered in [11–16]. In these differential games a pursuer with a defined detection region was pitted against an evader whose goal was to escape as soon as possible. The differential game studied by Dobbie and Taylor considered a fast pursuer with turn restrictions and circular surveillance region against a slower maneuverable evader capable of instantaneous changes in heading [11, 12]. Different to Taylor's work, Lewin imposed a turning rate constraint on the pursuer and allowed the pursuer's speed to vary from full stop to a bounded maximum [13, 14]. Another differential game investigated by Fuchs involved a fast pursuer that was pitted against a slower and less maneuverable evader with radar cross section [15]. In the game, the pursuer aimed to accumulate enough information about the target to achieve a defined probability of identification while the evader tried to evade the pursuer to remain undetected.

While the previous works have described optimal means of conducting ISR missions when the ISR platform is faster than the target, less common is the consideration of conducting ISR on targets which are faster. The capture of a faster ship by a slower one was proposed by Ogilvy [17] and solved by Klamkin. In an early work by Breakwell, a pursuit-evasion game was posed wherein a slower pursuer was employed against a faster evader [18]. Breakwell, also considered a nonzero capture radius for the slower pursuer. The approach taken by Breakwell solved for the acquisition of a faster evader by a slower pursuer, but ISR requires keeping the pursuer within the surveillance range of the pursuer for as long as possible. In [19] the observation of a faster target in 2-D was solved by Weintraub et al.; this paper is an extension of that work by considering the observation in the 3-D Cartesian space rather than restriction to a 2-D plane.

One motivation for considering the mobile target to be faster than the observer is for the modeling of air-to-air ISR missions. In the event that a slower ISR platform has made contact with a faster target, the strategy for the observer which maximizes the observation time is of interest. Using optimal control theory [20], this paper poses and solves for the optimal heading and flight path angle of a slower observer which results in max-time observation of the faster target in 3-D when simple motion is considered.

II. Optimal Control

Consider the optimal observation of a faster, non-maneuvering target by a slower observer in 3-D. Define the constant speed of the observer, O, and the target, T, as v_O and v_T respectively. The state space is composed of the position of the observer and the target whose locations in Cartesian space are $(x_O, y_O, z_O)^T$ and $(x_T, y_T, z_T)^T$ respectively. The complete state of the observation scenario, $\mathbf{x}$, is defined as follows:

$$\mathbf{x} = (x_O, y_O, z_O, x_T, y_T, z_T)^T \in \mathbb{R}^6 \tag{1}$$

The observer's control is composed of the instantaneous heading angle, ψ, and flight path angle, γ. The control vector, $\mathbf{u}$, is defined as follows:

$$\mathbf{u} = (\psi_O, \gamma_O)^T \in \mathbb{R}^2 \tag{2}$$

A governing assumption in this scenario is that the target is faster than the observer, $v_O < v_T$. Without loss of generality, the speed ratio between the observer and the target is defined as: $\mu = v_O/v_T$. In the scenario, the target is faster than the observer and therefore: $0 < \mu < 1$. Using normalization, the nonlinear dynamics, $\dot{\mathbf{x}}(t) = f(\mathbf{x}(t), \mathbf{u}(t), t)$,

may be represented as function of the speed ratio, μ, rather than their individual speeds as follows:

$$\begin{pmatrix} \dot{x}_O \\ \dot{y}_O \\ \dot{z}_O \\ \dot{x}_T \\ \dot{y}_T \\ \dot{z}_T \end{pmatrix} = \begin{pmatrix} \mu \cos\gamma_O \cos\psi_O \\ \mu \cos\gamma_O \sin\psi_O \\ \mu \sin\gamma_O \\ \cos\gamma_T \cos\psi_T \\ \cos\gamma_T \sin\psi_T \\ \sin\gamma_T \end{pmatrix} \tag{3}$$

In the model, it is assumed that the position and course of the target is constant and known by the observer. As described in Eq. (3), the course of the target is defined by the target's heading, ψ_T, and flight path angle, γ_T. The control of the observer is his heading, $\psi \in [0, 2\pi)$, and flight path angle, $\gamma \in [-\pi, \pi]$. At the onset we consider the target to be a distance R from the observer. Also, the observer is located at an azimuth, β, and elevation, α with respect to the target's position at the instant the scenario begins. More explicitly:

$$\overline{TO} = R \quad |t = t_0 \tag{4}$$

The initial conditions in the scenario are shown in Figure 1. This spherical model assumes that observation is guaranteed so long as the target is within a fixed range of the observer, independent of the agent's respective azimuth and elevation to each other. In this paper we consider the time-optimal strategy of the observer, O which maximizes the time the faster target is kept under observation.

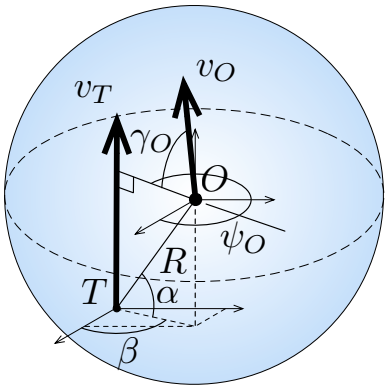

Fig. 1 The initial geometry when the observer has made contact with the target

Since the target is faster than the observer, escape from the circular observation envelope is guaranteed. Moreover, the termination set which represents the escape of the target from the observation circle is defined as follows:

$$\mathscr{C} = \{\mathbf{x} | R^2 - (x_O - x_T)^2 - (y_O - y_T)^2 - (z_O - z_T)^2 \leq 0\} \tag{5}$$

The terminal time, t_f, is defined as the instant where the state and time satisfies Eq. (5); at which time, the terminal state is: $\mathbf{x}(t_f) = (x_{O_f}, y_{O_f}, z_{O_f}, x_{T_f}, y_{T_f}, z_{T_f})^T$. Since our objective is to maximize the time by which the target remains within the circular observation radius, we consider the max-time objective functional:

$$J = \int_0^{t_f} -1 \, \mathrm{d}t = -t_f \tag{6}$$

The optimal time of observation is $t_f^* = -\min J$ subject to the termination set in Eq. (5). The goal is to find the optimal observer's heading and flight path angle time histories which minimize the objective cost functional in Eq. (6), namely:

$$\mathbf{u}^* = \underset{\mathbf{u}}{\operatorname{argmin}} J \tag{7}$$

In this scenario, the Hamiltonian is defined as the inner product of the costates and the dynamics, $\mathscr{H} = \langle \boldsymbol{\lambda}, f(\mathbf{x}, \mathbf{u}, t) \rangle$. The Hamiltonian can be written more explicitly as follows:

$$\begin{aligned} \mathscr{H} =& \lambda_{x_O} \mu \cos\gamma_O \cos\psi_O + \lambda_{y_O} \mu \cos\gamma_O \sin\psi_O + \lambda_{z_O} \mu \sin\gamma_O \\ &+ \lambda_{x_T} \cos\gamma_T \cos\psi_T + \lambda_{y_T} \cos\gamma_T \sin\psi_T + \lambda_{z_T} \sin\gamma_T \end{aligned} \tag{8}$$

where the costates are $\boldsymbol{\lambda} = (\lambda_{x_O} \ \lambda_{y_O} \ \lambda_{z_O} \ \lambda_{x_T} \ \lambda_{y_T} \ \lambda_{z_T})^T$.

A. Necessary Conditions for Optimality:

Utilizing the Hamiltonian in Eq. (8), the necessary conditions for optimality are formulated by taking the following partial derivatives:

$$\dot{\mathbf{x}}^*(t) = \frac{\partial \mathscr{H}(\mathbf{x}^*(t), \boldsymbol{\lambda}^*(t), \boldsymbol{u}_O^*(t), t)}{\partial \boldsymbol{\lambda}^*(t)} \tag{9}$$

$$\dot{\boldsymbol{\lambda}}^*(t) = -\frac{\partial \mathscr{H}(\mathbf{x}^*(t), \boldsymbol{\lambda}^*(t), \boldsymbol{u}_O^*(t), t)}{\partial \mathbf{x}^*(t)} \tag{10}$$

$$\mathbf{0} = \frac{\partial \mathscr{H}(\mathbf{x}^*(t), \boldsymbol{\lambda}^*(t), \boldsymbol{u}_O^*(t), t)}{\partial \boldsymbol{u}_O^*(t)} \tag{11}$$

where the superscript, $*$, represents optimally. Evaluating the necessary condition described in Eq. (11):

$$\begin{pmatrix} 0 \\ 0 \end{pmatrix} = \begin{pmatrix} \frac{\partial \mathscr{H}}{\partial \psi_O} \\ \frac{\partial \mathscr{H}}{\partial \gamma_O} \end{pmatrix} = \begin{pmatrix} -\lambda_{x_O}^* \mu \cos\gamma_O^* \sin\psi_O^* + \lambda_{y_O}^* \mu \cos\gamma_O^* \cos\psi_O^* \\ -\lambda_{x_O}^* \mu \sin\gamma_O^* \cos\psi_O^* - \lambda_{y_O}^* \mu \sin\gamma_O^* \sin\psi_O^* + \lambda_{z_O}^* \mu \cos\gamma_O^* \end{pmatrix} \tag{12}$$

Algebraic manipulation of the first term in Eq. (12) provides a relationship between the optimal heading of the observer and the costates for the observer.

$$0 = -\lambda_{x_O}^* \mu \cos\gamma_O^* \sin\psi_O^* + \lambda_{y_O}^* \mu \cos\gamma_O^* \cos\psi_O^* \tag{13}$$

Through algebraic manipulation Eq. (13) can be simplified to be the following:

$$\cos^2\psi_O^* = \frac{\lambda_{x_O}^{*2}}{\lambda_{x_O}^{*2} + \lambda_{y_O}^{*2}} \tag{14}$$

Using the trigonometric identity $\sin^2(x) + \cos^2(x) = 1 \ \forall x \in \mathbb{R}$, Eq. (14) can be written as follows:

$$\sin^2\psi_O^* = \frac{\lambda_{y_O}^{*2}}{\lambda_{x_O}^{*2} + \lambda_{y_O}^{*2}} \tag{15}$$

The derivation for reaching Equations (14) and (15) from Eq. (13) can be found in Appendix A.A. The following equation:

$$\begin{aligned} 0 &= -\lambda_{x_O}^* \mu \cos\gamma_O^* \sin\psi_O^* + \lambda_{y_O}^* \mu \cos\gamma_O^* \cos\psi_O^* \\ &= \cos\gamma_O^* \left(-\lambda_{x_O}^* \sin\psi_O^* + \lambda_{y_O}^* \cos\psi_O^* \right), \end{aligned}$$

implies that either $\cos\gamma_O^* = 0$, or, more generally $\left(-\lambda_{x_O}^* \sin\psi_O^* + \lambda_{y_O}^* \cos\psi_O^* \right) = 0$. The general case can be written

$$0 = \begin{bmatrix} \lambda_{y_O}^* & -\lambda_{x_O}^* \end{bmatrix} \cdot \begin{bmatrix} \sin\psi_O^* & \cos\psi_O^* \end{bmatrix},$$

which implies that the two vectors are perpendicular. Therefore, the optimal observer heading angle obeys the following:

$$\cos\psi_O^* = \pm \frac{\lambda_{x_O}}{\sqrt{\lambda_{x_O}^2 + \lambda_{y_O}^2}}, \qquad \sin\psi_O^* = \pm \frac{\lambda_{y_O}}{\sqrt{\lambda_{x_O}^2 + \lambda_{y_O}^2}}, \tag{16}$$

wherein the signs of the two expressions are coupled.

Similarly, though algebraic manipulation of the second term from Eq. (12), the optimal flight path angle of the observer is found as a function of the optimal costates of the observer. The second term from Eq. (12) is repeated here for convenience:

$$0 = -\lambda^*_{x_O}\mu \sin\gamma^*_O \cos\psi^*_O - \lambda^*_{y_O}\mu \sin\gamma^*_O \sin\psi^*_O + \lambda^*_{z_O}\mu \cos\gamma^*_O \tag{17}$$

Through algebraic manipulation Eq. (17) can be manipulated to obtain the following:

$$\cos^2\gamma^*_O = \frac{(\lambda^*_{x_O}\cos\psi^*_O + \lambda^*_{y_O}\sin\psi^*_O)^2}{\lambda^{*2}_{z_O} + (\lambda^*_{x_O}\cos\psi^*_O + \lambda^*_{y_O}\sin\psi^*_O)^2} \tag{18}$$

Further expansion and substitution of Equations (14) and (15) into Eq. (18), the optimal flight path angle as a function of the optimal costates is obtained:

$$\cos^2\gamma^*_O = \frac{\lambda^{*2}_{x_O} + \lambda^{*2}_{y_O}}{\lambda^{*2}_{x_O} + \lambda^{*2}_{y_O} + \lambda^{*2}_{z_O}} \tag{19}$$

The algebraic derivation which starts with Eq. (17) and results in Eq. (19) can be found in Appendix A.B. Further evaluation of the necessary conditions for optimality shows that the optimal heading and flight path angle by the observer is constant for the entire engagement. Evaluating the necessary condition in Eq. (10) one finds the dynamics of the costates by evaluating the following partials:

$$\begin{pmatrix} \dot\lambda^*_{x_O} \\ \dot\lambda^*_{y_O} \\ \dot\lambda^*_{z_O} \\ \dot\lambda^*_{x_T} \\ \dot\lambda^*_{y_Y} \\ \dot\lambda^*_{z_T} \end{pmatrix} = -\begin{pmatrix} \frac{\partial\mathscr{H}}{\partial x_O} \\ \frac{\partial\mathscr{H}}{\partial y_O} \\ \frac{\partial\mathscr{H}}{\partial z_O} \\ \frac{\partial\mathscr{H}}{\partial x_T} \\ \frac{\partial\mathscr{H}}{\partial y_T} \\ \frac{\partial\mathscr{H}}{\partial z_T} \end{pmatrix} = \begin{pmatrix} 0 \\ 0 \\ 0 \\ 0 \\ 0 \\ 0 \end{pmatrix} \tag{20}$$

Since the states are not explicit in the Hamiltonian in Eq. (8), the optimal costates are constant, i.e. $\boldsymbol{\lambda^*}(t) = \boldsymbol{\lambda^*}$ because the observer is holonomic. Since the optimal costates are constant, the optimal control is constant. Therefore the resulting optimal trajectory of the observer is a straight-line trajectory:

$$\psi^*_O(t) = \psi^*_O = \cos^{-1}\left(\sqrt{\frac{\lambda^{*2}_{x_O}}{\lambda^{*2}_{x_O} + \lambda^{*2}_{y_O}}}\right) \tag{21}$$

$$\gamma^*_O(t) = \gamma^*_O = \cos^{-1}\left(\sqrt{\frac{\lambda^{*2}_{x_O} + \lambda^{*2}_{y_O}}{\lambda^{*2}_{x_O} + \lambda^{*2}_{y_O} + \lambda^{*2}_{z_O}}}\right) \tag{22}$$

B. Transversality Conditions

Next, consider the transversality conditions which may be used to formulate the relationship between the states and costates at final time:

$$\frac{\partial h}{\partial \mathbf{x}}(\mathbf{x}^*(t_f), t_f) - \boldsymbol{\lambda}^*(t_f) = d\frac{\partial m}{\partial \mathbf{x}}(\mathbf{x}^*(t_f), t_f) \tag{23}$$

Define $h(\mathbf{x}(t_f), t_f)$ as the terminal cost of the objective functional, $\boldsymbol{\lambda}(t_f)$ as the costates at final time, d as a slack variable, and $m(\mathbf{x}(t_f), t_f)$ as the terminal manifold. From Eq. (6), the terminal cost in the objective cost functional is constant, $\frac{\partial h}{\partial \mathbf{x}} = 0$. We defined the terminal manifold in Eq. (5) and therefore:

$$m(\mathbf{x}^*(t_f), t_f) = \left(x^*_O(t_f) - x^*_T(t_f)\right)^2 + \left(y^*_O(t_f) - y^*_T(t_f)\right)^2 + \left(z^*_O(t_f) - z^*_T(t_f)\right)^2 - R^2 \tag{24}$$

Substitution of Eq. (24) in to the transversality condition Eq. (23) the following is obtained:

$$-\boldsymbol{\lambda}^*(t_f) = d\begin{pmatrix} \frac{\partial m}{\partial x_O} & \frac{\partial m}{\partial y_O} & \frac{\partial m}{\partial z_O} & \frac{\partial m}{\partial x_T} & \frac{\partial m}{\partial y_T} & \frac{\partial m}{\partial z_T} \end{pmatrix}^T \tag{25}$$

Therefore:

$$\begin{pmatrix} \lambda^*_{x_O} \\ \lambda^*_{y_O} \\ \lambda^*_{z_O} \\ \lambda^*_{x_T} \\ \lambda^*_{y_T} \\ \lambda^*_{z_T} \end{pmatrix} = -d \begin{pmatrix} \frac{\partial m}{\partial x_O} \\ \frac{\partial m}{\partial y_O} \\ \frac{\partial m}{\partial z_O} \\ \frac{\partial m}{\partial x_T} \\ \frac{\partial m}{\partial y_T} \\ \frac{\partial m}{\partial z_T} \end{pmatrix} = 2d \begin{pmatrix} x_{T_f} - x_{O_f} \\ y_{T_f} - y_{O_f} \\ z_{T_f} - z_{O_f} \\ x_{O_f} - x_{T_f} \\ y_{O_f} - y_{T_f} \\ z_{O_f} - z_{T_f} \end{pmatrix} \tag{26}$$

Substitution of the costates from Eq. (26) into the optimal control from Equations (21) and (22) the optimal heading and flight path angle of the observer may be formulated as a function of the final observer and target state as follows:

$$\cos\psi^*_O = \pm\sqrt{\frac{\left(2d(x_{T_f} - x_{O_f})\right)^2}{\left(2d(x_{T_f} - x_{O_f})\right)^2 + \left(2d(y_{T_f} - y_{O_f})\right)^2}}, \qquad \sin\psi^*_O = \pm\sqrt{\frac{\left(2d\left(y_{T_f} - y_{O_f}\right)\right)^2}{\left(2d\left(x_{T_f} - x_{O_f}\right)\right)^2 + \left(2d\left(y_{T_f} - y_{O_f}\right)\right)^2}} \tag{27}$$

$$\cos\gamma^*_O = \pm\sqrt{\frac{\left(2d(x_{T_f} - x_{O_f})\right)^2 + \left(2d(y_{T_f} - y_{O_f})\right)^2}{\left(2d(x_{T_f} - x_{O_f})\right)^2 + \left(2d(y_{T_f} - y_{O_f})\right)^2 + \left(2d(z_{T_f} - z_{O_f})\right)^2}} \tag{28}$$

Simplifying Equations (27) and (28), one is able to eliminate the slack variable and find the resulting optimal heading and flight path angle at final time as a function of the final observer and target states:

$$\cos\psi^*_O = \pm\frac{(x_{T_f} - x_{O_f})}{\sqrt{(x_{T_f} - x_{O_f})^2 + (y_{T_f} - y_{O_f})^2}}, \qquad \sin\psi^*_O = \pm\frac{(y_{T_f} - y_{O_f})}{\sqrt{(x_{T_f} - x_{O_f})^2 + (y_{T_f} - y_{O_f})^2}} \tag{29}$$

$$\cos\gamma^*_O(t_f) = \pm\frac{\sqrt{(x_{T_f} - x_{O_f})^2 + (y_{T_f} - y_{O_f})^2}}{R} \tag{30}$$

From Equations (29) and (30) we see that the angle from the observer to the target at final time is either the same as the optimal heading or anti-parallel. The latter case is clearly suboptimal since the observer would be aimed directly away from the target at final time. Thus, the sign ambiguity in Equations (29) and (30) may be eliminated. An illustration of the optimal engagement is shown in Figure 2.

III. Main Result

Provided the target's heading, flight path angle, and speed the optimal heading and flight path angle of the observer which maximizes the time of observation of a non-maneuverable target can be analytically obtained. Without loss of generality, the observer-target scenario is rotated about the target such that the target velocity is aligned with the vertical axis as shown in Figure 2.

A. Optimal Observer Heading

Because the headings of both agents are constant, the plane formed by the points T, O, and S is invariant – it remains perpendicular to the (x, y)-plane. From Eq. (29), the optimal observer heading is aimed directly towards the (x, y) projection of the target. Thus the optimal heading of the observer which maximizes observation time is: $\psi^*_O = \beta + \pi$, where β is the (constant) azimuth of the observer w.r.t. the target.

B. Optimal Observer Flight Path Angle

Consider the triangle formed from $\triangle OST$. A drawing of the full geometry is shown in Figure 2. Using the law of cosines the following the following equation describes the relationship between the range between the observer to target at final time ($\overline{OS}$), the path by which the target is observed ($\overline{TS}$), the observation radius (R), and the elevation angle when observation is first made (α):

$$\overline{OS}^2 = \overline{TS}^2 + R^2 - 2R\overline{TS}\cos(\pi/2 - \alpha) \tag{31}$$

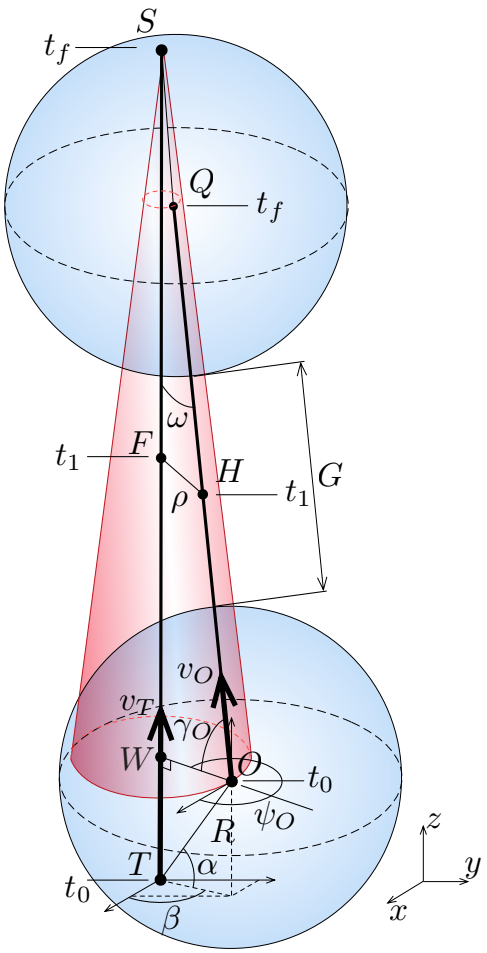

Fig. 2 The Observation Scenario in 3-D

Using the speed ratio between the observer and the target the distance traversed by the observer over the engagement is proportional to the distance traversed by the target: $\overline{OQ} = \mu\overline{TS}$, and therefore:

$$\overline{OS} = \mu\overline{TS} + R \tag{32}$$

Substitution of Eq. (32) into Eq. (31) and recognizing that $\cos(\pi/2 - x) = \sin x \ \forall x \in \mathbb{R}$, the following is obtained:

$$\left(\mu\overline{TS} + R\right)^2 = \overline{TS}^2 + R^2 - 2R\overline{TS}\sin\alpha \tag{33}$$

Through algebraic manipulation, Eq. (33) may be solved for $\overline{TS}$. The derivation is shown in Appendix A.C.

$$\overline{TS} = \frac{2R(\mu + \sin\alpha)}{1 - \mu^2} \tag{34}$$

Next, the optimal the path angle is solved using triangle $\triangle OWS$. Recognizing that the Cosine of an angle in a right triangle is equal to the adjacent leg over the hypotenuse:

$$\cos\gamma_O^* = \frac{R\cos\alpha}{\overline{OS}} \tag{35}$$

Substitution of Equations (32) and (34) into Eq. (35) the optimal flight path is derived and shown in Appendix A.D. The resulting optimal flight path angle is as follows:

$$\gamma_O^* = \cos^{-1}\left(\frac{(1 - \mu^2)\cos\alpha}{\mu^2 + 2\mu\sin\alpha + 1}\right) \tag{36}$$

Special Case: $\alpha \equiv \pi/2$

When the elevation angle from the Target to the Observer, α, is $\pi/2$, the observer is directly in front of the path of travel of the target. Substitution of $\alpha \equiv \pi/2$ in Eq. (36), the optimal flight path angle,$\gamma_O^* = \pi/2$, as expected.

IV. Observation Invariance

It is important to show that once the target is within the observation range of the observer, R, that the target remains within the observation range until the termination set is reached. Figure 2 shows the geometry for the optimal two-agent scenario. In order to prove that the target stays within the observation range of the observer, define the two-norm range between the observer and target: $\rho(t) = \sqrt{(x_O(t) - x_T(t))^2 + (y_O(t) - y_T(t))^2 + (z_O(t) - z_T(t))^2} \; \forall \; t \in (t_0, t_f)$.

Utilizing the Law of Cosines to analyze $\triangle OST$, the following relationship is obtained:

$$\overline{TO}^2 = \overline{TS}^2 + (\overline{OQ} + \overline{QS})^2 - 2\overline{TS}(\overline{OQ} + \overline{QS}) \cos\omega \tag{37}$$

Recognize that $\overline{OT} = R$, $\overline{QS} = R$, and $\overline{TS} = \mu\overline{OQ}$. Substitution into Eq. (37), the following is obtained:

$$R^2 = \overline{TS}^2 + (\mu\overline{TS} + R)^2 - 2\overline{TS}(\mu\overline{TS} + R) \cos\omega \tag{38}$$

Expanding and solving Eq. (38) for $\cos\omega$:

$$\cos\omega = \frac{\overline{TS}(1+\mu) + 2\mu R}{2(\mu\overline{TS} + R)} \tag{39}$$

Now consider a future time, $t_1 \in (t_0, t_f)$. Using the Law of Cosines for $\triangle FHS$:

$$\rho^2 = \overline{FS}^2 + \overline{HS}^2 - 2\overline{FS}\;\overline{HS} \cos\omega \tag{40}$$

Recognize that $\overline{HQ} = \mu\overline{FS}$ and $\overline{HS} = \overline{HQ} + R$. Substituting these into Eq. (40):

$$\rho^2 = \overline{FS}^2 + (\mu\overline{FS} + R)^2 - 2\overline{FS}(\mu\overline{FS} + R) \cos\omega \tag{41}$$

Substitution of Eq. (39) into Eq. (41), the following is obtained:

$$\rho^2 = \overline{FS}^2 + (\mu\overline{FS} + R)^2 - 2\overline{FS}(\mu\overline{FS} + R)\frac{\overline{TS}(1+\mu) + 2\mu R}{2(\mu\overline{TS} + R)} \tag{42}$$

Algebraic manipulation of Eq. (42) results in the following:

$$\rho^2 = R^2 + \frac{\overline{FS}R}{(\mu\overline{TS} + R)}\left(\overline{FS} - \overline{TS}\right)\left(1 - \mu^2\right) \tag{43}$$

Notice in Eq. (43) the sign of the individual terms.

$$\rho^2 = R^2 + \underbrace{\frac{\overline{FS}R}{(\mu\overline{TS} + R)}}_{\text{Positive}} \underbrace{\left(\overline{FS} - \overline{TS}\right)}_{\text{Negative}} \underbrace{\left(1 - \mu^2\right)}_{\text{Positive}} \tag{44}$$

Therefore, for values of $t_1 \in (t_0, t_f)$, $\rho < R$, and therefore once the target is within the observation range of the observer, he stays there under optimal play until the terminal set is reached at t_f.

V. Observation Manifold

The function which describes the target distance while being observed can be found in Eq. (34). The target distance while being observed is a function of the elevation from the target to the observer at initial time, α, the radius of

observation, R, and the speed ratio, μ. Because velocity is normalized with respect to the target, the range $\overline{TS} = v_T t = t$. Substituting the time of exposure, t into Eq. (34), the polar equation for exposure time is as following:

$$t_f = \frac{2R(\mu + \sin\alpha)}{1 - \mu^2} \tag{45}$$

Plotting the time of exposure as a function of the target to the observer elevation angle, α, produces a limaçon whose cusp is located at the target location. Utilizing Eq. (45), the angle which describes the range of headings the target could take which result in a zero-observation time (ZOT). Note that the boundary for zero-time of exposure solutions exist when $t_f = 0$. From Eq. (45), values of α which result in non-positive values of t_f represent angles for which the observation time is zero. Thus, setting the length $t_f \leq 0$ in Eq. (45), one obtains the conditions for zero time of exposure:

$$\frac{2R}{1 - \mu^2}(\mu + \sin\alpha) \leq 0 \tag{46}$$

From Eq. (46), the regions wherein the observer is unable to observe the target occur when the angle α lies in the following range:

$$\alpha_{\text{ZOT}} \in \left[-\frac{\pi}{2},\ -\sin^{-1}\mu\right] \tag{47}$$

Assuming the observer implements the optimal heading which maximized observation time of the faster target, eq. Eq. (34) can be algebraically manipulated to provide the observer-target headings which guarantee a desired observation time. The following is the equation which describes the angle α which guarantees the desired observation time, t.

$$\alpha = \cos^{-1}\left(\frac{2\mu R - (1 - \mu^2)t}{2R}\right) \tag{48}$$

It should be noted that the guarantees for observation time are bounded by

$$t \in \left[0,\ \frac{2R(\mu + 1)}{1 - \mu^2}\right] \tag{49}$$

VI. Example

An illustration of the maximum observation of a slower target in 3-D is presented in this section. In this example, the observer is endowed with an observation radius of $R = 2$. The observer is half as fast as the target and as a result, the speed ratio is $\mu = 0.5$. Consider the target vehicle to be moving with a flight path angle of $\pi/2$ rad and heading of 0 rad. Define the azimuth to be $\pi/3$ rad and the elevation of the observer with respect to the target to be $\pi/3$ rad. From Eq. (36), the optimal flight path angle is calculated to be ≈ 1.3926 rad. And the heading is selected to point toward the target, and therefore is 4.1888 rad. Using the optimal flight path angle and heading, Figure 3 shows the maximum time observation scenario in 3-D.

In the figure, the observer's path is represented by the blue line, the observation radius is represented by the shaded blue sphere, and the faster target is represented by the red line. The initial locations are not filled-in and the final time locations of both agents are solid.

In order to ensure observation of the target by the observer, the instantaneous range between the two agents would need to be less than or equal to the observation radius, R. We find in Figure 4 that, in fact, the instantaneous range between the observer and the target is less than or equal to the observation range of the observer for the entire engagement.

For various elevation angles, α, we see the possible observation time in Figure 5 when the observer implements his optimal strategy. The figure is shown in both polar and Cartesian form for the sake of presenting the angular and time information easier. Note that observation time is independent of azimuth since β does not appear in Eq. (45) and therefore only plots for various elevation angles are presented.

In Figure 5, the red lines represent zero-time of exposure while blue lines represent positive non-zero time of exposure. By plotting the observation time for all possible elevation angles, α, we see that maximum observation occurs when the target and observer move co-linear with one another ($\alpha = \pi/2$) as expected. From Figure 5, one may observe the zero-exposure time angles as well as the exposure time limaçon. For our example, the zero-time observation angle is found by computing Eq. (47). In our example, the zero time of exposure occurs between $\alpha \in [-\pi/2, -\pi/6]$ rad.

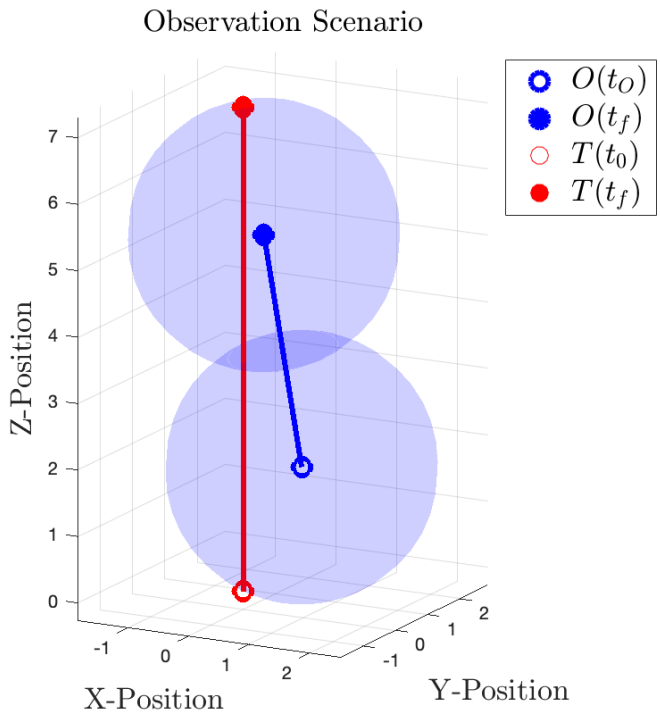

Fig. 3 The maximum-time observation of a faster Target by a slower Observer in 3-D Cartesian Space

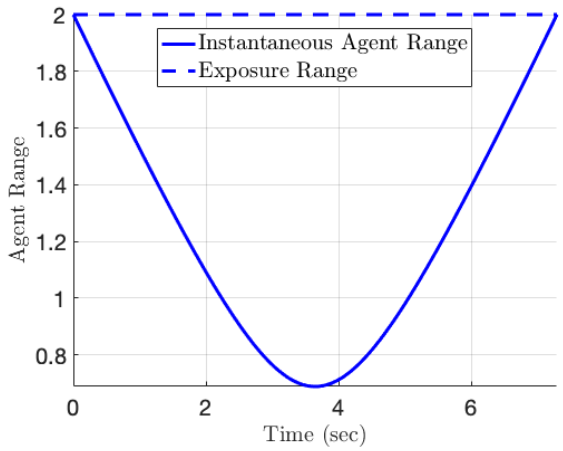

Fig. 4 The instantaneous range is inside the exposure region for the entirely of the scenario

VII. Conclusions / Future Work

In conclusion, using a spherical region centered at the observer and commanding the instantaneous heading and flight path angle of the observer, we have maximized the time by which the target remains inside the observation range. Using the calculus of variations and optimal control theory, we have posed and solved for the optimal instantaneous heading and flight path angle of the observer required to maximize the observation of a faster non-maneuvering target. First, we showed that the optimal heading and flight path angle of the observer are constant. Next, we showed that the observation time is independent of initial azimuth angle and dependent upon the relative elevation angle, observation radius, and speed ratio. Using the relations for exposure time, the regions where observation is not possible are described. Finally, we presented an example which highlights the maximum observation of a non-maneuvering faster target by a

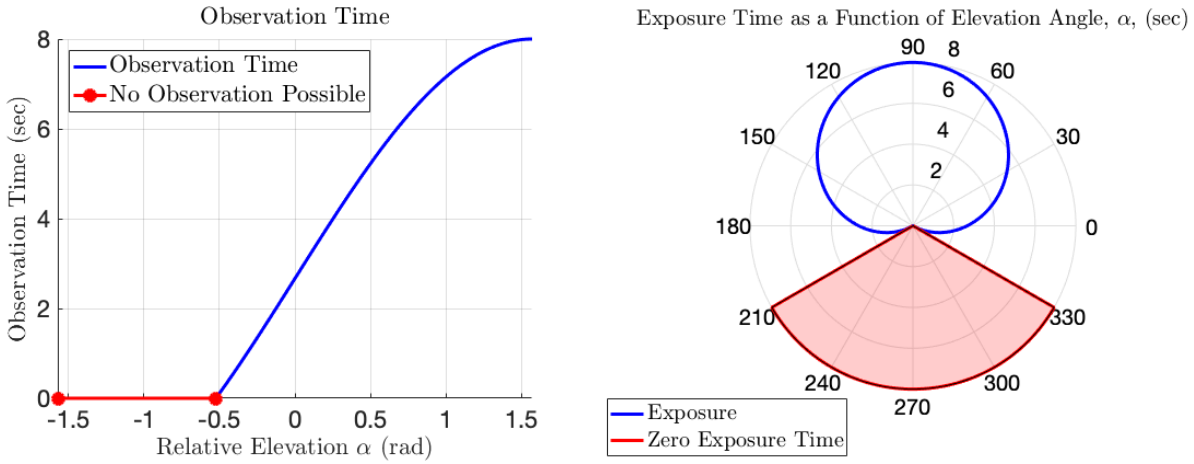

Fig. 5 The relationship of the observation time as a function of the relative elevation angle, α, shown in both Cartesian and Polar plots

slower observer. The figures presented in the example illustrate the findings and demonstrate the results of this work.

Future work of interest includes non-straight target paths. This includes and is not limited to, target paths which are circular, elliptic, or composed of straight and curved sections. Of course, arbitrary target paths are also of interest. However, the tractability of closed form solutions for maximum observation for arbitrary target paths is unlikely. It is hypothesized that numeric methods may be leveraged in order to determine optimal observer strategies when the target maneuvers arbitrarily; this is left for future investigation.

A. Select Derivations

A. Optimal Heading as a Function of Optimal Costates

This derivation starts with Eq. (13) and derives Equations (14) and (15) through algebraic manipulation.

$$
\begin{aligned}
0 &= -\lambda^*_{x_O}\mu\cos\gamma^*_O\sin\psi^*_O + \lambda^*_{y_O}\mu\cos\gamma^*_O\cos\psi^*_O \\
0 &= -\lambda^*_{x_O}\sin\psi^*_O + \lambda^*_{y_O}\cos\psi^*_O \\
\lambda^*_{x_O}\sin\psi^*_O &= \lambda^*_{y_O}\cos\psi^*_O \\
\lambda^{*2}_{x_O}\sin^2\psi^*_O &= \lambda^{*2}_{y_O}\cos^2\psi^*_O \\
\lambda^{*2}_{x_O}(1-\cos^2\psi^*_O) &= +\lambda^{*2}_{y_O}\cos^2\psi^*_O \\
\lambda^{*2}_{x_O} - \lambda^{*2}_{x_O}\cos^2\psi^*_O &= \lambda^{*2}_{y_O}\cos^2\psi^*_O \\
\lambda^{*2}_{x_O} &= (\lambda^{*2}_{x_O} + \lambda^{*2}_{y_O})\cos^2\psi^*_O \\
\cos^2\psi^*_O &= \frac{\lambda^{*2}_{x_O}}{\lambda^{*2}_{x_O} + \lambda^{*2}_{y_O}}
\end{aligned}
$$

$$
1-\sin^2\psi^*_O = \frac{\lambda^{*2}_{x_O}}{\lambda^{*2}_{x_O} + \lambda^{*2}_{y_O}} \Rightarrow \sin^2\psi^*_O = \frac{\lambda^{*2}_{y_O}}{\lambda^{*2}_{x_O} + \lambda^{*2}_{y_O}}
$$

B. Optimal Flight Path Angle as a Function of Optimal Costates

This derivation starts with Eq. (17) and derives Eq. (19) through algebraic manipulation.

$$
\begin{aligned}
0 &= -\lambda^*_{x_O}\mu\sin\gamma^*_O\cos\psi^*_O - \lambda^*_{y_O}\mu\sin\gamma^*_O\sin\psi^*_O + \lambda^*_{z_O}\mu\cos\gamma^*_O \\
0 &= -\lambda^*_{x_O}\sin\gamma^*_O\cos\psi^*_O + \lambda^*_{y_O}\sin\gamma^*_O\sin\psi^*_O + \lambda^*_{z_O}\cos\gamma^*_O \\
0 &= -\sin\gamma^*_O(\lambda^*_{x_O}\cos\psi^*_O + \lambda^*_{y_O}\sin\psi^*_O) + \lambda^*_{z_O}\cos\gamma^*_O \\
\sin\gamma^*_O(\lambda^*_{x_O}\cos\psi^*_O + \lambda^*_{y_O}\sin\psi^*_O) &= \lambda^*_{z_O}\cos\gamma^*_O \\
\sin^2\gamma^*_O(\lambda^*_{x_O}\cos\psi^*_O + \lambda^*_{y_O}\sin\psi^*_O)^2 &= \lambda^{*2}_{z_O}\cos^2\gamma^*_O \\
(1-\cos^2\gamma^*_O)(\lambda^*_{x_O}\cos\psi^*_O + \lambda^*_{y_O}\sin\psi^*_O)^2 &= \lambda^{*2}_{z_O}\cos^2\gamma^*_O \\
(\lambda^*_{x_O}\cos\psi^*_O + \lambda^*_{y_O}\sin\psi^*_O)^2 - \cos^2\gamma^*_O(\lambda^*_{x_O}\cos\psi^*_O + \lambda^*_{y_O}\sin\psi^*_O)^2 &= \lambda^{*2}_{z_O}\cos^2\gamma^*_O \\
(\lambda^*_{x_O}\cos\psi^*_O + \lambda^*_{y_O}\sin\psi^*_O)^2 &= \cos^2\gamma^*_O(\lambda^*_{x_O}\cos\psi^*_O + \lambda^*_{y_O}\sin\psi^*_O)^2 + \lambda^{*2}_{z_O}\cos^2\gamma^*_O \\
(\lambda^*_{x_O}\cos\psi^*_O + \lambda^*_{y_O}\sin\psi^*_O)^2 &= \cos^2\gamma^*_O((\lambda^*_{x_O}\cos\psi^*_O + \lambda^*_{y_O}\sin\psi^*_O)^2 + \lambda^{*2}_{z_O})
\end{aligned}
$$

Therefore:

$$
\cos^2\gamma^*_O = \frac{(\lambda^*_{x_O}\cos\psi^*_O + \lambda^*_{y_O}\sin\psi^*_O)^2}{\lambda^{*2}_{z_O} + (\lambda^*_{x_O}\cos\psi^*_O + \lambda^*_{y_O}\sin\psi^*_O)^2}
$$

Expanding further and substitution of Equations (14) and (15) for $\cos^2\psi^*_O$ and $\sin^2\psi^*_O$:

$$
\begin{aligned}
\cos^2\gamma^*_O &= \frac{(\lambda^*_{x_O}\cos\psi^*_O + \lambda^*_{y_O}\sin\psi^*_O)^2}{\lambda^{*2}_{z_O} + (\lambda^*_{x_O}\cos\psi^*_O + \lambda^*_{y_O}\sin\psi^*_O)^2} \\
&= \frac{\lambda^{*2}_{x_O}\cos^2\psi^*_O + \lambda^{*2}_{y_O}\sin^2\psi^*_O + 2\lambda^*_{x_O}\lambda^*_{y_O}\cos\psi^*_O\sin\psi^*_O}{\lambda^{*2}_{z_O} + \lambda^{*2}_{x_O}\cos^2\psi^*_O + \lambda^{*2}_{y_O}\sin^2\psi^*_O + 2\lambda^*_{x_O}\lambda^*_{y_O}\cos\psi^*_O\sin\psi^*_O} \\
&= \frac{\lambda^{*2}_{x_O}\left(\frac{\lambda^{*2}_{x_O}}{\lambda^{*2}_{x_O}+\lambda^{*2}_{y_O}}\right) + \lambda^{*2}_{y_O}\left(\frac{\lambda^{*2}_{y_O}}{\lambda^{*2}_{x_O}+\lambda^{*2}_{y_O}}\right) + 2\lambda^*_{x_O}\lambda^*_{y_O}\left(\frac{\lambda^{*2}_{x_O}}{\lambda^{*2}_{x_O}+\lambda^{*2}_{y_O}}\right)^{1/2}\left(\frac{\lambda^{*2}_{y_O}}{\lambda^{*2}_{x_O}+\lambda^{*2}_{y_O}}\right)^{1/2}}{\lambda^{*2}_{z_O} + \lambda^{*2}_{x_O}\left(\frac{\lambda^{*2}_{x_O}}{\lambda^{*2}_{x_O}+\lambda^{*2}_{y_O}}\right) + \lambda^{*2}_{y_O}\left(\frac{\lambda^{*2}_{y_O}}{\lambda^{*2}_{x_O}+\lambda^{*2}_{y_O}}\right) + 2\lambda^*_{x_O}\lambda^*_{y_O}\left(\frac{\lambda^{*2}_{x_O}}{\lambda^{*2}_{x_O}+\lambda^{*2}_{y_O}}\right)^{1/2}\left(\frac{\lambda^{*2}_{y_O}}{\lambda^{*2}_{x_O}+\lambda^{*2}_{y_O}}\right)^{1/2}}
\end{aligned}
$$

As an aside:

$$
2\lambda^*_{x_O}\lambda^*_{y_O}\left(\frac{\lambda^{*2}_{x_O}}{\lambda^{*2}_{x_O}+\lambda^{*2}_{y_O}}\right)^{1/2}\left(\frac{\lambda^{*2}_{y_O}}{\lambda^{*2}_{x_O}+\lambda^{*2}_{y_O}}\right)^{1/2} = 2\frac{\lambda^{*2}_{x_O}\lambda^{*2}_{y_O}}{\lambda^{*2}_{x_O}+\lambda^{*2}_{x_O}}
$$

Therefore $\cos^2\gamma_O$ may be written as:

$$
\begin{aligned}
\cos^2\gamma^*_O &= \frac{\lambda^{*2}_{x_O}\left(\frac{\lambda^{*2}_{x_O}}{\lambda^{*2}_{x_O}+\lambda^{*2}_{y_O}}\right) + \lambda^{*2}_{y_O}\left(\frac{\lambda^{*2}_{y_O}}{\lambda^{*2}_{x_O}+\lambda^{*2}_{y_O}}\right) + 2\frac{\lambda^{*2}_{x_O}\lambda^{*2}_{y_O}}{\lambda^{*2}_{x_O}+\lambda^{*2}_{x_O}}}{\lambda^{*2}_{z_O} + \lambda^{*2}_{x_O}\left(\frac{\lambda^{*2}_{x_O}}{\lambda^{*2}_{x_O}+\lambda^{*2}_{y_O}}\right) + \lambda^{*2}_{y_O}\left(\frac{\lambda^{*2}_{y_O}}{\lambda^{*2}_{x_O}+\lambda^{*2}_{y_O}}\right) + 2\frac{\lambda^{*2}_{x_O}\lambda^{*2}_{y_O}}{\lambda^{*2}_{x_O}+\lambda^{*2}_{x_O}}} \\
&= \frac{\lambda^{*2}_{x_O}\lambda^{*2}_{x_O} + \lambda^{*2}_{y_O}\lambda^{*2}_{y_O} + 2\lambda^{*2}_{x_O}\lambda^{*2}_{y_O}}{\lambda^{*2}_{z_O} + \lambda^{*2}_{x_O}\lambda^{*2}_{x_O} + \lambda^{*2}_{y_O}\lambda^{*2}_{y_O} + 2\lambda^{*2}_{x_O}\lambda^{*2}_{y_O}}
\end{aligned}
$$

Also as an aside:

$$
\frac{(\lambda^{*2}_{x_O} + \lambda^{*2}_{y_O})(\lambda^{*2}_{x_O} + \lambda^{*2}_{y_O})}{\lambda^{*2}_{x_O} + \lambda^{*2}_{y_O}} = \frac{\lambda^{*2}_{x_O}\lambda^{*2}_{x_O} + \lambda^{*2}_{y_O}\lambda^{*2}_{y_O} + 2\lambda^{*2}_{x_O}\lambda^{*2}_{y_O}}{\lambda^{*2}_{x_O} + \lambda^{*2}_{y_O}}
$$

$$
\frac{(\lambda^{*2}_{x_O} + \lambda^{*2}_{y_O})(\lambda^{*2}_{x_O} + \lambda^{*2}_{y_O})}{\lambda^{*2}_{x_O} + \lambda^{*2}_{y_O}} - \frac{2\lambda^{*2}_{x_O}\lambda^{*2}_{y_O}}{\lambda^{*2}_{x_O} + \lambda^{*2}_{y_O}} = \frac{\lambda^{*2}_{x_O}\lambda^{*2}_{x_O} + \lambda^{*2}_{y_O}\lambda^{*2}_{y_O}}{\lambda^{*2}_{x_O} + \lambda^{*2}_{y_O}}
$$

Therefore $\cos^2\gamma_O$ may be written as:

$$\cos^2\gamma_O^* = \frac{\frac{(\lambda_{x_O}^{*2}+\lambda_{y_O}^{*2})(\lambda_{x_O}^{*2}+\lambda_{y_O}^{*2})}{\lambda_{x_O}^{*2}+\lambda_{y_O}^{*2}}}{\lambda_{z_O}^{*2}+\frac{(\lambda_{x_O}^{*2}+\lambda_{y_O}^{*2})(\lambda_{x_O}^{*2}+\lambda_{y_O}^{*2})}{\lambda_{x_O}^{*2}+\lambda_{y_O}^{*2}}} = \frac{\frac{(\lambda_{x_O}^{*2}+\lambda_{y_O}^{*2})(\lambda_{x_O}^{*2}+\lambda_{y_O}^{*2})}{\lambda_{x_O}^{*2}+\lambda_{y_O}^{*2}}}{\lambda_{z_O}^{*2}\frac{\lambda_{x_O}^{*2}+\lambda_{y_O}^{*2}}{\lambda_{x_O}^{*2}+\lambda_{y_O}^{*2}}+\frac{(\lambda_{x_O}^{*2}+\lambda_{y_O}^{*2})(\lambda_{x_O}^{*2}+\lambda_{y_O}^{*2})}{\lambda_{x_O}^{*2}+\lambda_{y_O}^{*2}}}$$

$$= \frac{(\lambda_{x_O}^{*2}+\lambda_{y_O}^{*2})(\lambda_{x_O}^{*2}+\lambda_{y_O}^{*2})}{\lambda_{z_O}^{*2}(\lambda_{x_O}^{*2}+\lambda_{y_O}^{*2})+(\lambda_{x_O}^{*2}+\lambda_{y_O}^{*2})(\lambda_{x_O}^{*2}+\lambda_{y_O}^{*2})}$$

Therefore:

$$\cos^2\gamma_O^* = \frac{\lambda_{x_O}^{*2}+\lambda_{y_O}^{*2}}{\lambda_{x_O}^{*2}+\lambda_{y_O}^{*2}+\lambda_{z_O}^{*2}}$$

C. Optimal Path of Target Exposure, $\overline{TS}$

The derivation of the target exposure length starts with Eq. (33) and derives Eq. (34) through algebraic manipulation.

$$\left(\mu\overline{TS}+R\right)^2 = \overline{TS}^2 + R^2 - 2R\overline{TS}\cos(\pi/2-\alpha)$$

Recall that $\cos(\pi/2-x) = sin(x)\ \forall\ x\in\mathbb{R}$. Therefore the equation is simplified as follows:

$$\left(\mu\overline{TS}+R\right)^2 = \overline{TS}^2 + R^2 - 2R\overline{TS}\sin(\alpha)$$

Expanding all terms in the equation the following is obtained:

$$\mu^2\overline{TS}^2 + R^2 + 2R\mu\overline{TS} = \overline{TS}^2 + R^2 - 2R\overline{TS}\sin(\alpha)$$

Removing R^2 from both sides:

$$\mu^2\overline{TS}^2 + 2R\mu\overline{TS} = \overline{TS}^2 - 2R\overline{TS}\sin(\alpha)$$

Divide both sides of the equation by $\overline{TS}$:

$$\mu^2\overline{TS} + 2R\mu = \overline{TS} + 2R\cos(\alpha)$$

$$(1-\mu^2)\overline{TS} = 2R(\mu+\sin\alpha)$$

Therefore:

$$\overline{TS} = \frac{2R(\mu+\sin\alpha)}{1-\mu^2}$$

D. Optimal Flight Path Angle

Substitution of Equations (32) and (34) into Eq. (35) the optimal flight path angle in Eq. (36) is derived. Starting with Eq. (35):

$$\cos\gamma_O^* = \frac{R\cos\alpha}{\overline{OS}}$$

Substitution of Eq. (32) for $\overline{OS}$ the following is obtained

$$\cos\gamma_O^* = \frac{R\cos\alpha}{\mu\overline{TS}+R}$$

Further, substitution of Eq. (34) for $\overline{TS}$, the following is obtained:

$$\cos\gamma_O^* = \frac{R\cos\alpha}{\mu(\frac{2R(\mu+\sin\alpha)}{1-\mu^2})+R} = \frac{R\cos\alpha}{\frac{2R\mu(\mu+\sin\alpha)}{1-\mu^2}+R} = \frac{R\cos\alpha}{\frac{2R\mu(\mu+\sin\alpha)}{1-\mu^2}+R\frac{1-\mu^2}{1-\mu^2}}$$

$$= \frac{(1-\mu^2)R\cos\alpha}{2R\mu(\mu+\sin\alpha)+R(1-\mu^2)} = \frac{(1-\mu^2)\cos\alpha}{2\mu(\mu+\sin\alpha)+(1-\mu^2)} = \frac{(1-\mu^2)\cos\alpha}{2\mu^2+2\mu\sin\alpha+1-\mu^2}$$

$$= \frac{(1-\mu^2)\cos\alpha}{\mu^2+2\mu\sin\alpha+1}$$

Therefore

$$\gamma_O^* = \cos^{-1}\left(\frac{(1-\mu^2)\cos\alpha}{\mu^2 + 2\mu\sin\alpha + 1}\right)$$

Acknowledgments

The views expressed are those of the author and do not reflect the official policy or position of the US Air Force, Department of Defense or the US Government. This research was made possible do to the facilities and resources made available at Air Force Research Laboratory. Approved for public release: distribution unlimited. (88ABW-2020-2486).

References

[1] Henry, D. J., "ISR Systems: Past, Present, and Future," *Airborne Intelligence, Surveillance, Reconnaissance (ISR) Systems and Applications XIII*, Vol. 9828, SPIE, Baltimore, MD, 2016, p. 982802. https://doi.org/10.1117/12.2229443.

[2] Kent, B. M., and Ehret, R. A., "Rethinking Intelligence, Surveillance, and Reconnaissance in a Wireless Connected World," *IEEE Antennas and Propagation Society, AP-S International Symposium (Digest)*, IEEE, Chicago, IL, 2012, p. 2. https://doi.org/10.1109/APS.2012.6348961.

[3] Wilkins, M., and Marchelli, T., "An Optimal Approach to Unmanned Maritime Surveillance Analysis," *12th AIAA/ISSMO Multidisciplinary Analysis and Optimization Conference*, American Institute of Aeronautics and Astronautics (AIAA), Victoria, British Columbia, Canada, 2012, pp. 1–7. https://doi.org/10.2514/6.2008-5835.

[4] Shaferman, V., and Shima, T., "Unmanned Aerial Vehicles Cooperative Tracking of Moving Ground Target in Urban Environments," *Journal of Guidance, Control, and Dynamics*, Vol. 31, No. 5, 2008, pp. 1360–1371. https://doi.org/10.2514/1.33721, URL https://doi.org/10.2514/1.33721.

[5] He, R., Bachrach, A., and Roy, N., "Efficient Planning Under Uncertainty for a Target-Tracking Micro-Aerial Vehicle," *Proceedings - IEEE International Conference on Robotics and Automation*, IEEE, Anchorage, AK, 2010, pp. 1–8. https://doi.org/10.1109/ROBOT.2010.5509548.

[6] Wettergren, T. A., and Traweek, C. M., "The Search Benefits of Autonomous Mobility in Distributed Sensor Networks," *International Journal of Distributed Sensor Networks*, Vol. 2012, No. 2, 2012, p. 11. https://doi.org/10.1155/2012/797040.

[7] Liu, B., Dousse, O., Nain, P., and Towsley, D., "Dynamic Coverage of Mobile Sensor Networks," *IEEE Transactions on Parallel and Distributed Systems*, Vol. 24, No. 2, 2013, pp. 301–311. https://doi.org/10.1109/TPDS.2012.141.

[8] Livermore, R. A., "Optimal UAV Path Planning for Tracking a Moving Ground Vehicle With a Gimbaled Camera," M.S. Thesis. Air Force Institute of Technology, 2014, pp. 1–106. URL https://scholar.afit.edu/etd/751/.

[9] Zhang, C., and Hwang, I., "Multiple Maneuvering Target Tracking Using a Single Unmanned Aerial Vehicle," *Journal of Guidance, Control, and Dynamics*, Vol. 42, No. 1, 2019, pp. 78–90. https://doi.org/10.2514/1.g002696, URL https://doi.org/10.2514/1.G002696.

[10] Garnett, R. J., and Flenner, A., "Optimal Control for Improved UAV Communication," *AIAA Scitech Forum*, American Institute of Aeronautics and Astronautics (AIAA), San Diego, CA, 2019, pp. 1–14. https://doi.org/10.2514/6.2019-0921.

[11] Dobbie, J. M., "Solution of Some Surveillance-Evasion Problems by Methids of Differential Games," *Proceedings of the 4th International Conference on Operational Research, MIT*, John Wiley and Sons, New York, New York, 1966, pp. 170–184.

[12] Taylor, J. G., "Application of Differential Games to Problems of Naval Warware: Surveillance-Evasion - Part 1," Tech. rep., United States Naval Postgraduate School, Monterey, CA, 1970. https://doi.org/10.4135/9781483359878.n684.

[13] Lewin, J., and Breakwell, J. V., "The Surveillance-Evasion Game of Degree," *Journal of Optimization Theory and Applications*, Vol. 16, No. 3-4, 1975, pp. 339–353. https://doi.org/10.1007/BF01262940.

[14] Lewin, J., and Olsder, G. J., "Conic Surveillance Evasion," *Journal of Optimization Theory and Applications*, Vol. 27, No. 1, 1979, pp. 107–125. https://doi.org/10.1007/BF00933329.

[15] Fuchs, Z. E., and Metcalf, J., "Equilibrium Radar-Target Interactions in an ATR Scenario: A Differential Game," *2018 IEEE Radar Conference, RadarConf 2018*, IEEE, Oklahoma City, OK, 2018, pp. 1228–1233. https://doi.org/10.1109/RADAR.2018.8378738.

[16] Patsko, V., Kumkov, S., and Turova, V., "Pursuit-Evasion Games," *Handbook of Dynamic Game Theory*, edited by Z. G. Basar T., Springer, Cham, 2018, pp. 1–87. https://doi.org/10.1007/978-3-319-44374-4{_}30.

[17] C. S. Ogilvy, M. S. K., "A Slow Ship Intercepting a Fast Ship," *The American Mathematical Monthly*, Vol. 59, No. 6, 1952, p. 408. https://doi.org/10.2307/2306820.

[18] Breakwell, J. V., "Pursuit of a Faster Evader," *The Theory and Application of Differential Games*, edited by J. D. Grote, Springer, Dordrecht, 1975, pp. 243–256. https://doi.org/10.1007/978-94-010-1804-3{_}22.

[19] Weintraub, I. E., Von Moll, A., Garcia, E., Casbeer, D., Demers, Z. J. L., and Pachter, M., "Maximum Observation of a Faster Non-Maneuvering Target by a Slower Observer," *American Control Conference (ACC)*, AACC, Denver, CO, 2020.

[20] Kirk, D. E., *Optimal Control Theory: An Introduction*, Dover Books on Electrical Engineering Series, Dover Publications, 2004.